Supplement of The Cryosphere, 20, 3025–3049, 2026
https://doi.org/10.5194/tc-20-3025-2026-supplement

The Cryosphere Open Access EGU

Supplement of

Mass changes of the Antarctic Peninsula ice sheet and peripheral glaciers, 2007–2021

Maud Bernat et al.

Correspondence to: Maud Bernat (maud.bernat@utoulouse.fr)

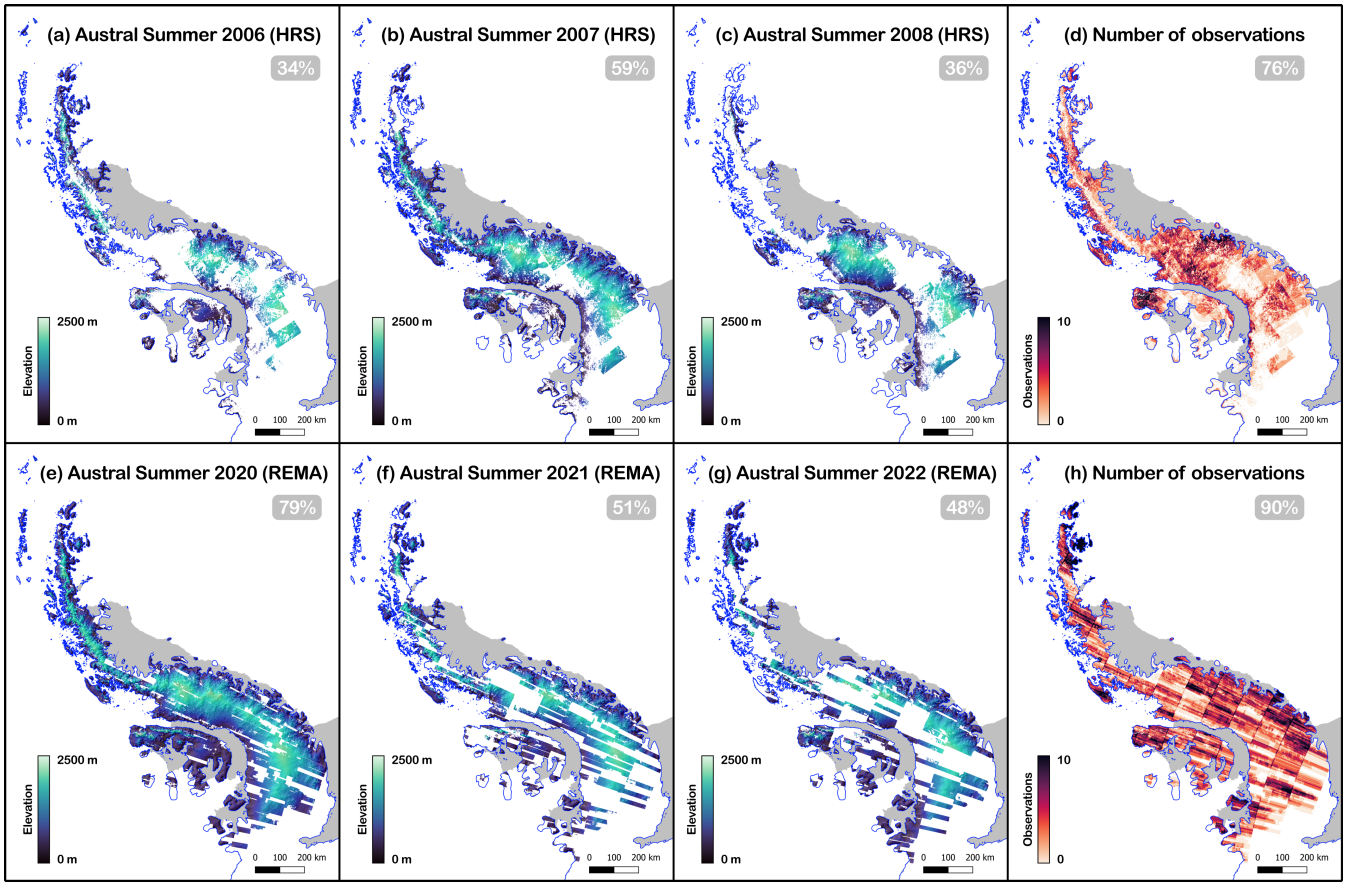

Figure S1. Spatial coverages of SPOT5-HRS segments and REMA DEMs. Spatial coverage of SPOT5-HRS segments for the austral summer 2006 (a), 2007 (b) and 2008 (c). Spatial coverage of REMA DEMs for the austral summer 2020 (e), 2021 (f) and 2022 (g). The total number of observations for each pixel is shown on panels (d) and (h). The percentage of the AP covered area is indicated in the upper right corner of each panel. The Bedmap3 outline of grounded ice is plotted in blue and the ice shelves are indicated in grey.

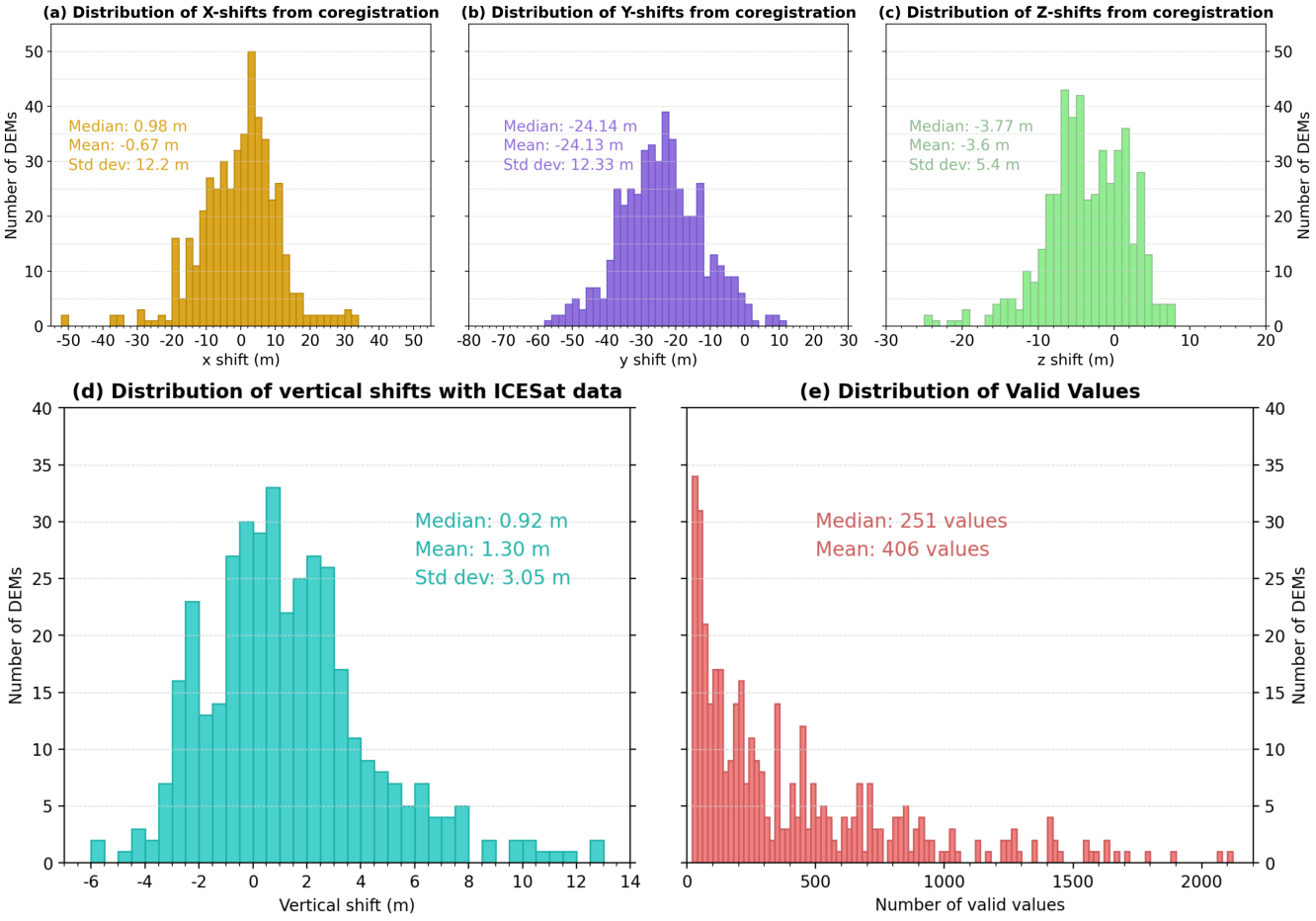

Figure S2. Statistical distributions of coregistration coefficients and vertical adjustment coefficients for HRS DEMs. (a) x-shifts, (b) y-shifts, (c) z-shifts, (d) vertical shift correction applied and (e) number of valid values used (at least 20 for the correction to be applied).

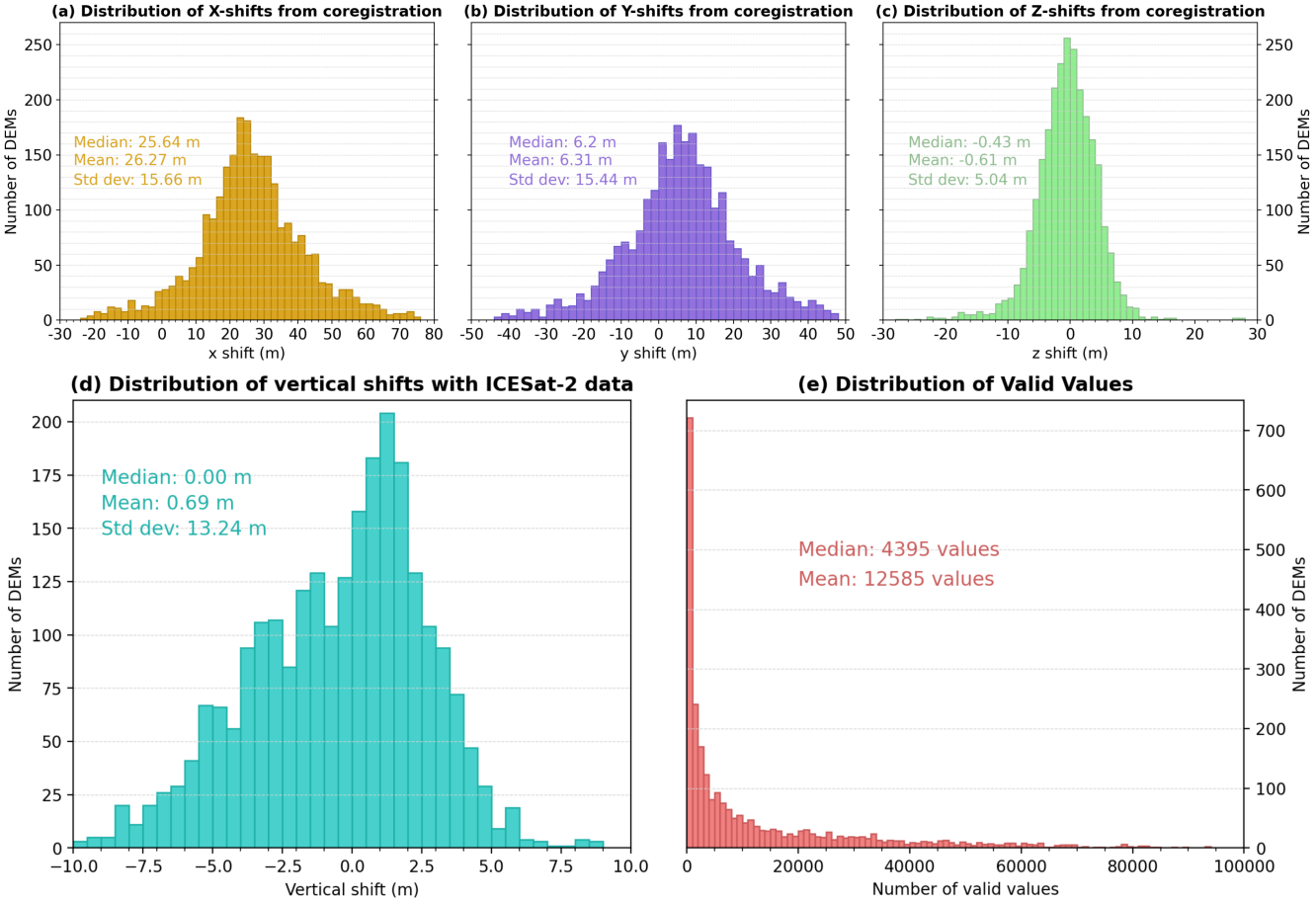

Figure S3. Statistical distributions of coregistration coefficients and vertical adjustment coefficients for REMA DEMs. (a) x-shifts, (b) y-shifts, (c) z-shifts, (d) vertical shift correction applied and (e) number of valid values used (at least 20 for the correction to be applied).

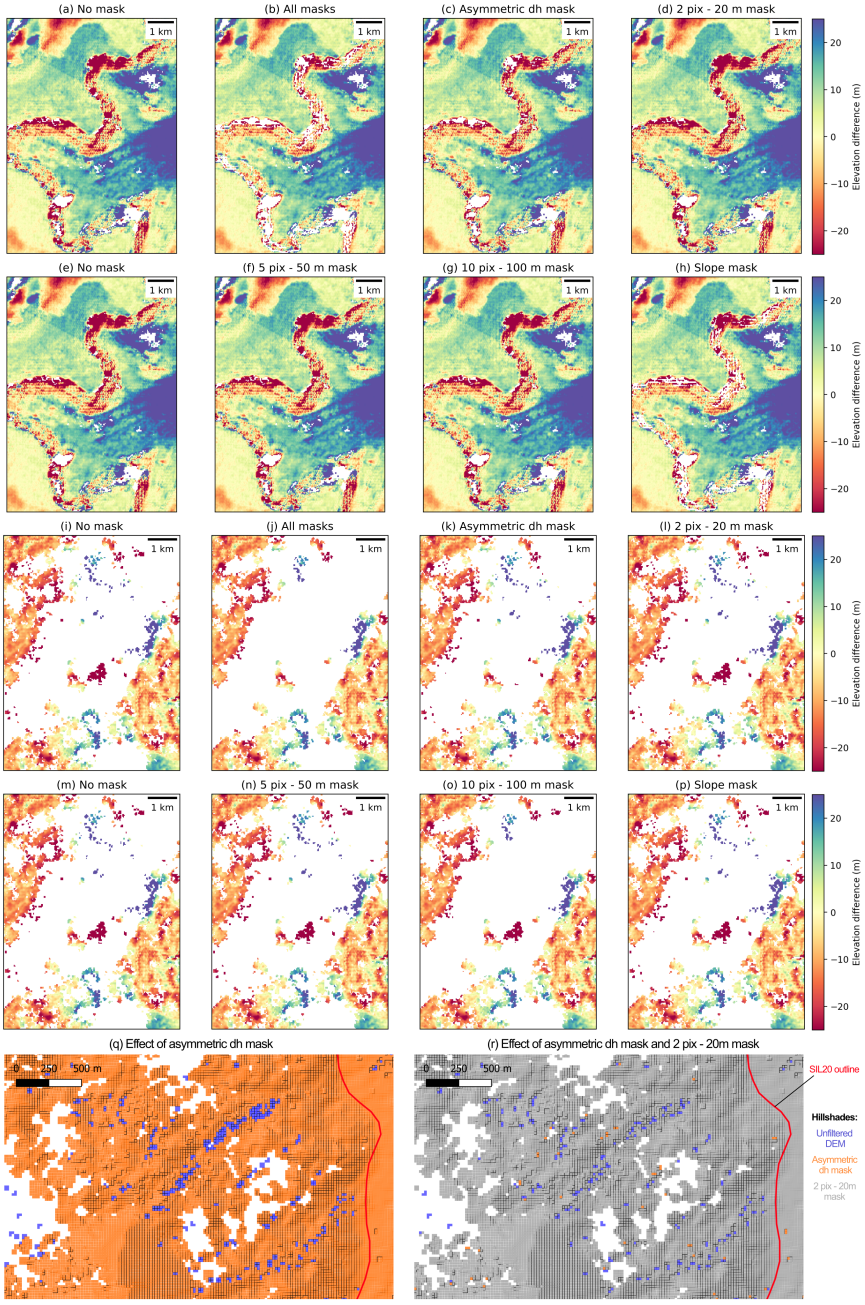

Figure S4. Three case studies of the different DEMs filters. The first zone, plotted on panels (a) to (h), justifies the use of the asymmetric dh mask (c) and the slope mask (h). The second zone illustrates the utility of the asymmetric dh mask (k) and the radius filters (o). The two bottom panels (q) and (r) show the fruitful combination of the asymmetric filter (orange hillshade) and the radius filter 2 pix - 20 m (grey hillshade) to remove pixel-scale aberrant values from the inital DEM (purple hillshade). The asymmetric filter removes a large part of the outliers (q) but the remaining ones are efficiently removed with the radius filter 2 pix - 20 m (r).

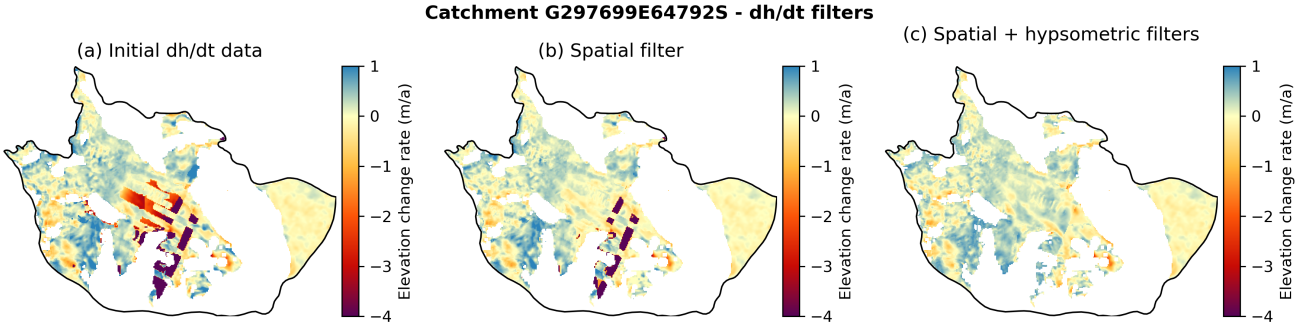

Figure S5. Effects of dh/dt filters on an example catchment. (a) Initial dh/dt data, (b) dh/dt data after spatial filtering, (c) dh/dt data after spatial and hypsometric filters.

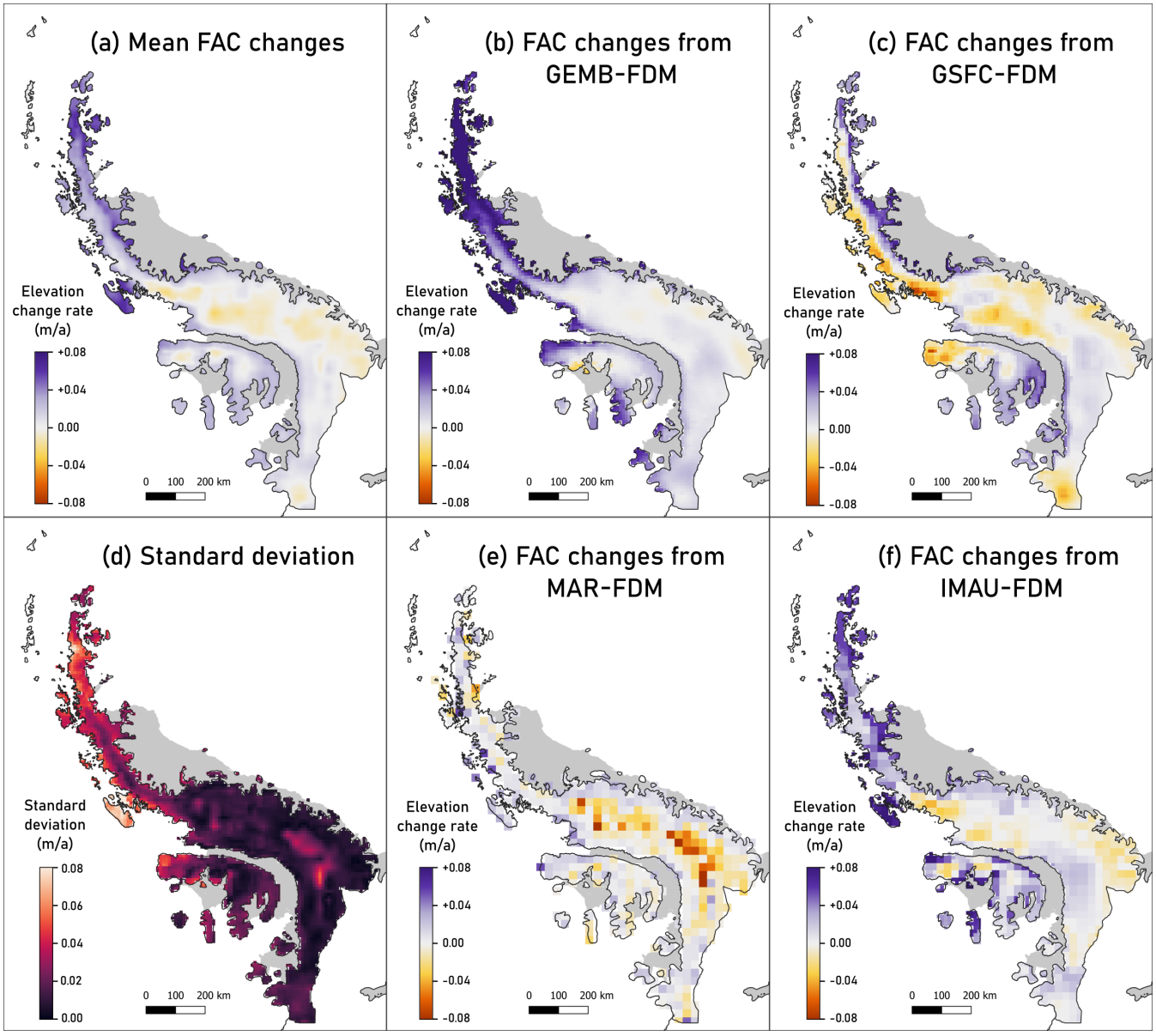

Figure S6. FAC elevation change rates from firn densification models (2007–2021). The mean FAC elevation change rate is shown on the (a), the standard deviation on (d) and the FAC elevation change rates coming from the different FDMs are plotted on (b), (c), (e) and (f).

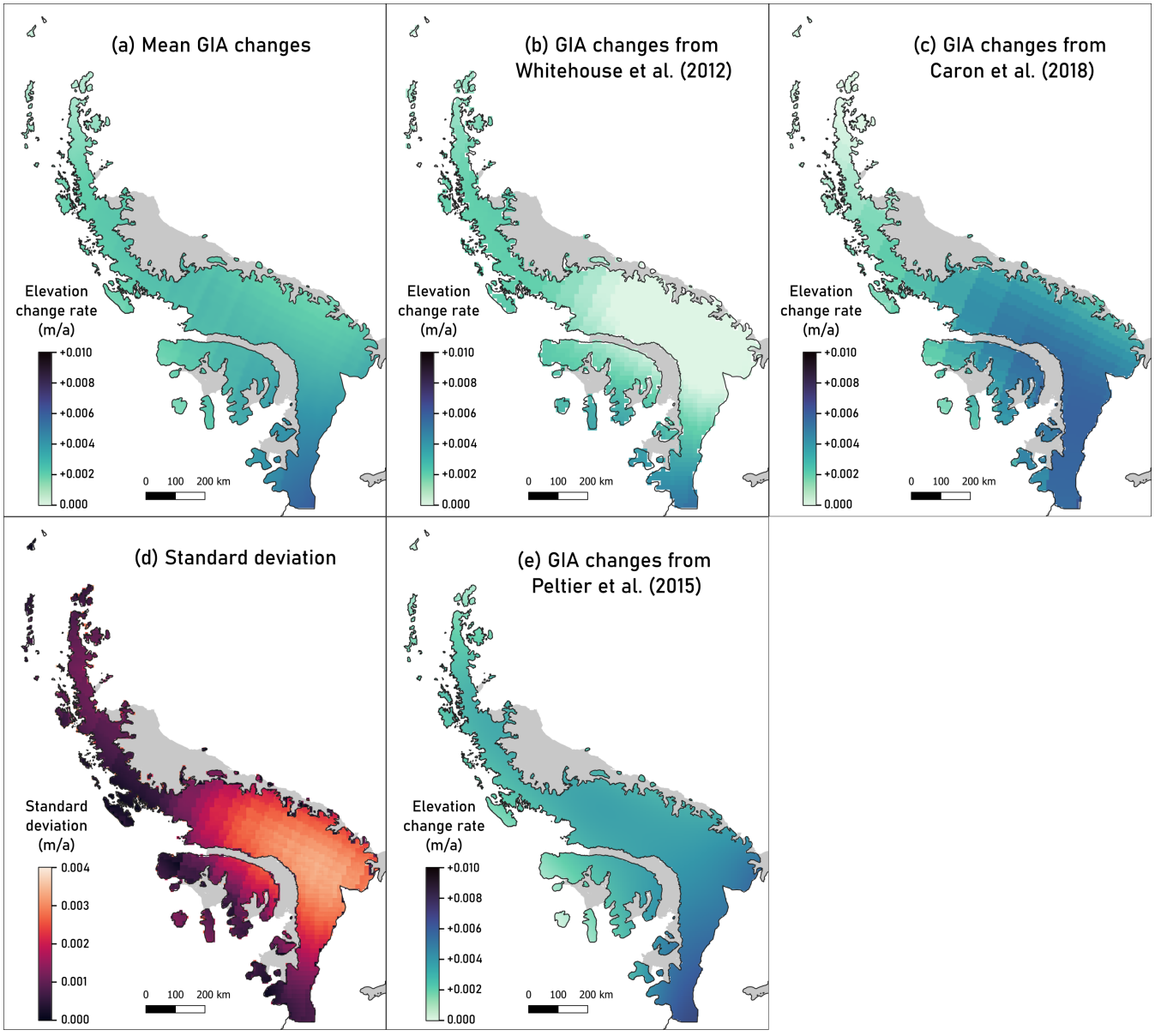

Figure S7. Elevation change rates from GIA models (2007−2021). The mean GIA elevation change rate is shown on (a), the standard deviation on (d) and the elevation change rates coming from the different models are plotted on (b), (c) and (e).

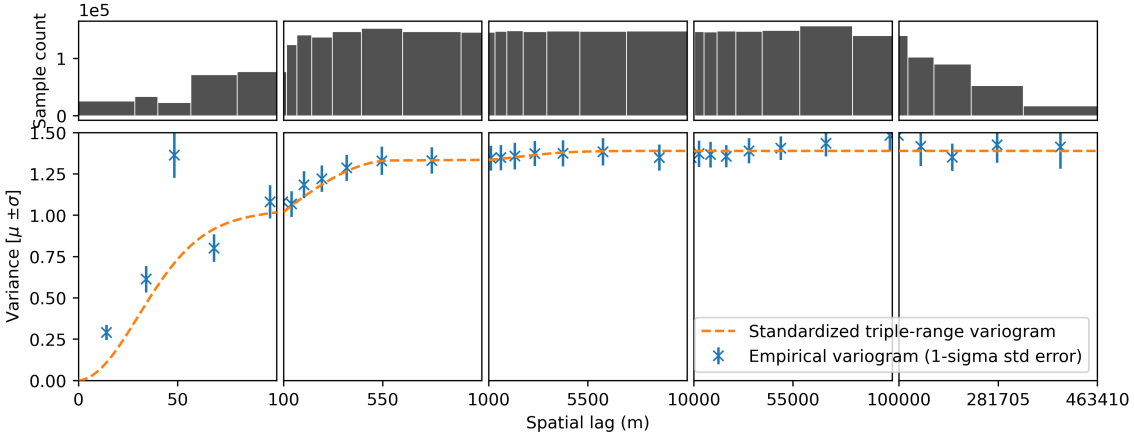

Figure S8. HRS variogram computed from the 13 HRS coincident pairs. The empirical variogram and the associated 1-σ standard deviation error is plotted in blue crosses. The modeled variogram based on the sum of three functions (two gaussians and a spherical) is shown in orange. The range and sill of the three ranges modeled are the following: range$_1$=86 m, sill$_1$ = 0.92 (spherical), range$_2$=596 m, sill$_2$ = 0.41 (gaussian) and range$_3$=6 523 m, sill$_3$ = 0.06 (gaussian).

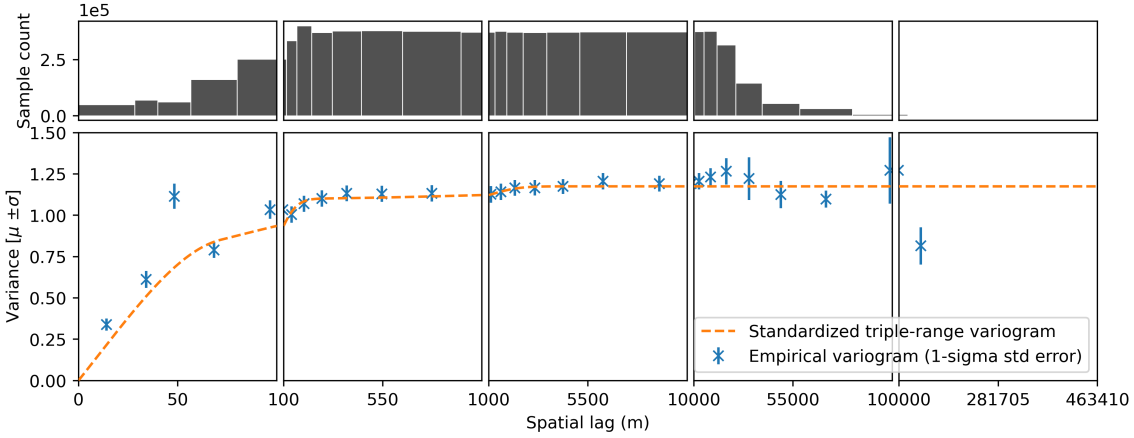

Figure S9. REMA variogram computed from the 23 REMA coincident pairs. The empirical variogram and the associated 1-σ standard deviation error is plotted in blue crosses. The modeled variogram based on the sum of three functions (two gaussians and a spherical) is shown in orange. The range and sill of the three ranges modeled are the following: range$_1$=71 m, sill$_1$ = 0.71 (spherical), range$_2$=217 m, sill$_2$ = 0.38 (gaussian) and range$_3$=3 342 m, sill$_3$ = 0.07 (gaussian).

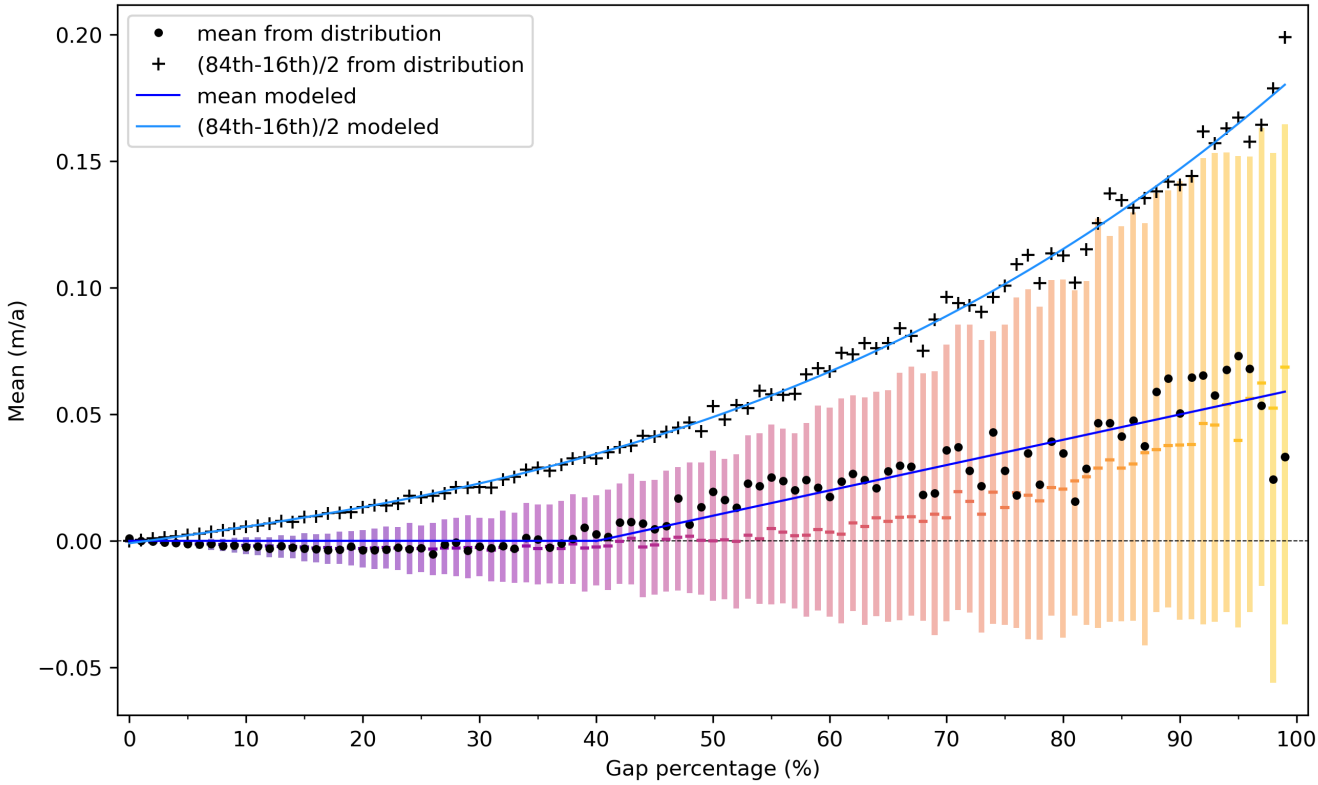

Figure S10. Relationship between the gap size in percentage of the total area and metrics of the mean difference between original and artificially voided dh/dt maps. For each gap size percent, the boxplot (median, 1^{st} and 3^{rd} quartiles) of the means is plotted in color. The mean is shown as a black dot and the robust dispersion metric (84^{th} percentile - 16^{th} percentile)/2 as a black cross. The piecewise-defined function fitted to the series of mean is shown in dark blue and the 3-degree polynomial function fitted to the robust dispersion metric series in light blue.

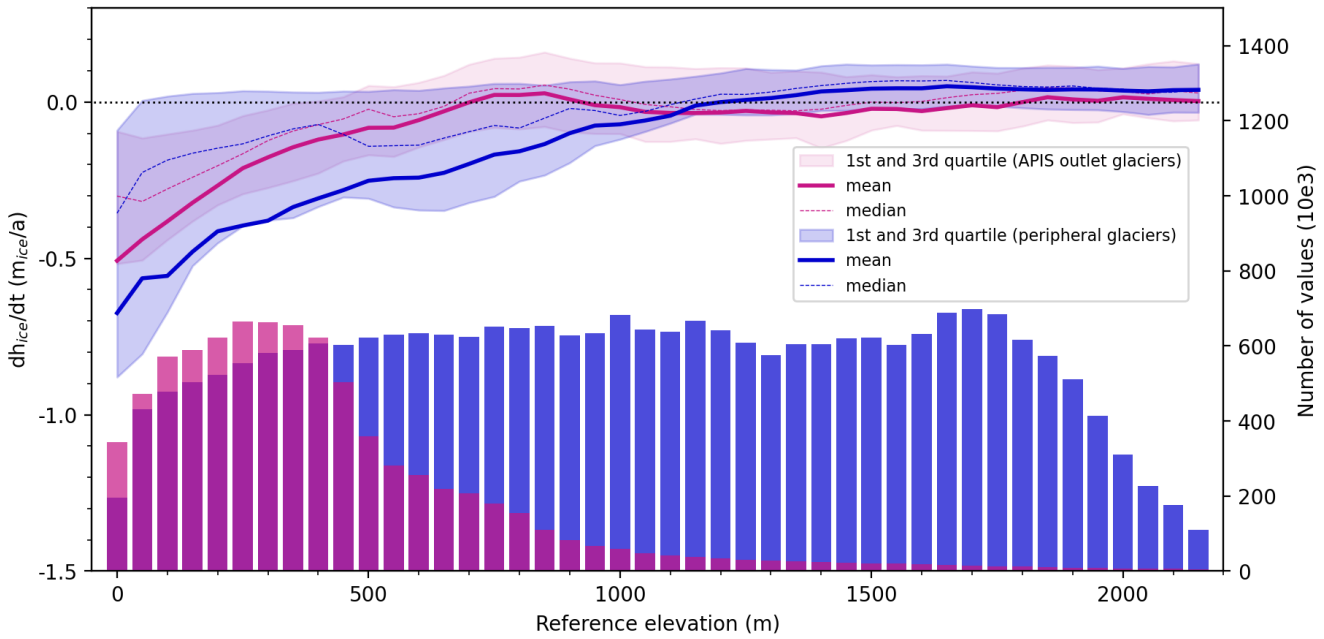

Figure S11. Hypsometric signal of ice elevation changes over the APIS (blue) and the peripheral glaciers (purple). For the two categories, the histograms at the bottom show the distribution of elevations. The distribution (median, mean, 1st and 3rd quartiles) of dh/dt values per elevation bin are plotted at the top.

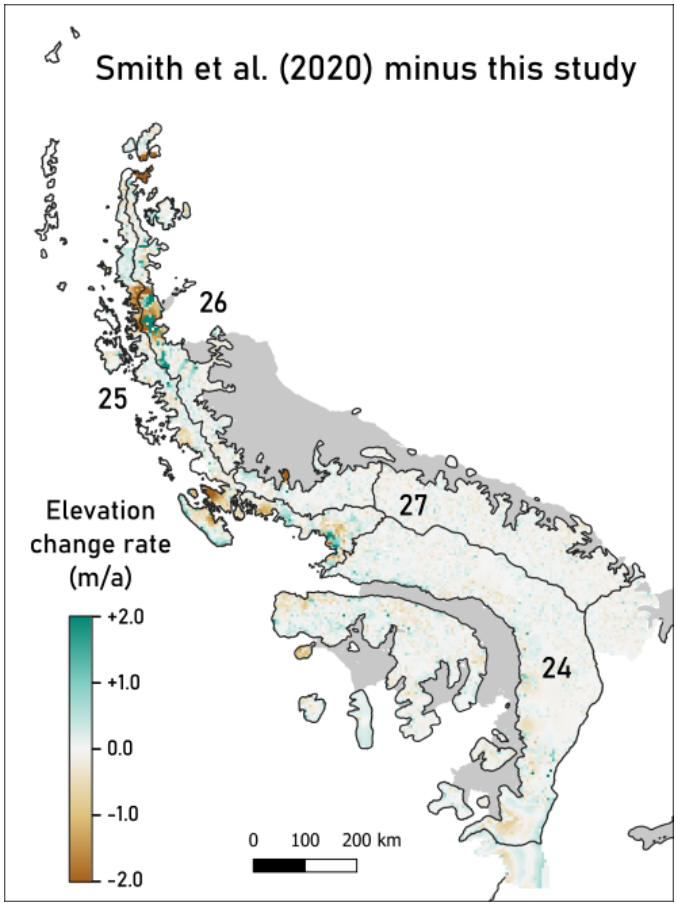

Figure S12. Elevation change rate difference between the elevation change map from ? and the one from this study. The ZWA12 outlines are plotted in black and the numbers correspond to the associated subregion number (24 to 27). The RGI outlines are plotted in black.

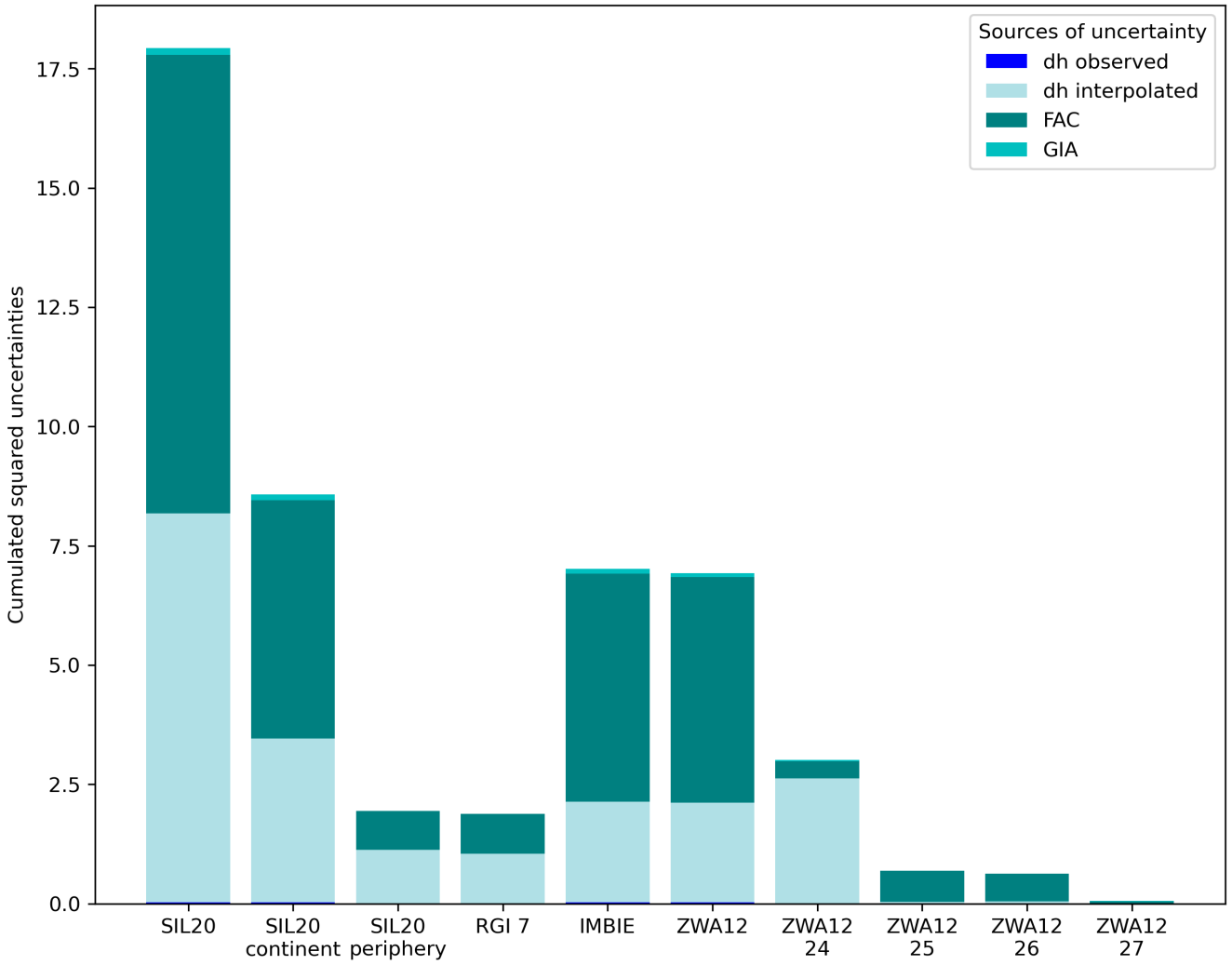

Figure S13. Contributions of sources of uncertainty for the main regions of the AP. For each outline, the different sources of uncertainties are plotted as a cumulative barplot.